Mansoura Engineering Journal

Volume 21 | Issue 3 Article 4

9-1-2021

Non-Newtonian Drag Reducing Fluid Flow in a Circular Pipe Filled with Porous Medium in the Non-Darcian Effects.

M. El-Kady
Mechanical Power Engineering Department., Faculty of Engineering., El-Mansoura University., Mansoura., Egypt., mselkady@mum.mans.eun.eg

M. Tolba
Mechanical Power Engineering Department., Faculty of Engineering., El-Mansoura University., Mansoura., Egypt.

L. Rabie
Mechanical Power Engineering Department., Faculty of Engineering., El-Mansoura University., Mansoura., Egypt.

Recommended Citation

El-Kady, M.; Tolba, M.; and Rabie, L. (2021) "Non-Newtonian Drag Reducing Fluid Flow in a Circular Pipe Filled with Porous Medium in the Non-Darcian Effects.," *Mansoura Engineering Journal*: Vol. 21 : Iss. 3 , Article 4.
Available at: https://doi.org/10.21608/bfemu.2021.152767

Non-Newtonian Drag Reducing Fluid Flow in a Circular Pipe Filled With Porous Medium in the non-Darcian Effects

سريان الموائع اللانيوتونية المخفضه للجر الاحتكاكى فى أنبوبة دائرية مملوءة بوسط مسامى تحت التأثيرات اللادارسيه

M.S. El-Kady, M.A. Tolba and L.H. Rabie

Mechanical Power Engineering Department
Mansoura University, Egypt

خلاصـــــه:

فى هذا البحث أجريت دراسة عددية ومعملية لسريان الموائع اللانيوتونيه (المخفضه للجر الاحتكاكى) فى مجرى دائرى مملوء بوسط مسامى. وقد تم تعديل معادلة دارسى-فورشهايمر-برينكمان لتأخذ فى الاعتبار تأثير اللزوجه الطولية اللانيوتونيه للمائع وكذلك التأثيرات اللادارسيه المختلفة مثل المسامية المتغيرة، التصور الداتى للمائع والاحتكاك اللزج عند الحوائط وتم حله باستخدام طريقه الفروق البسيطة. أجريت الدراسة النظرية على وسط مسامى دى حبيبات كرويه بقطر $d = 3.2$ mm ، وسبه قطر الحبيبات الكروية الى نصف قطر المجرى الدائرى $D = 0.32$ ، وقد تم دراسة السريان فى الوسط المسامى حتى رقم رينولدز Re يصل الى 10^5، معامل احتكاك لانيوتونى بمدى $0 \leq \psi \leq 5000$ ومعامل انحدار الضغط B يصل الى 10^{10}. وأظهرت النتائج أن التأثيرات اللانيوتونيه لها تأثيرا واضحا على شكل توزيع السرعة فى مقطع المجرى، وان تركيزات قليلة جدا من البوليمر يمكن أن تسبب نقص كبير فى السرعة المتوسطة للمائع وتعطى زيادة نسبيه فى السرعة فى المناطق الملاصقة للحائط مما يزيد من اندفاع سريان المائع فى هده المناطق. أعطت هذه الظاهرة بالتبعية تأثيرا ملحوظا على خصائص السريان مثل معامل الاحتكاك اللزج ومعامل الاحتكاك اللانيوتونى الناتج من اللزوجه الطولية ومن ثم على معامل الاحتكاك الكلى. وتعطى نتائج هده الدراسة تحليلا لسلوك كل من السرعة ومعاملات السريان للمائع واعتمادهما على معامل الاحتكاك اللانيوتونى. كما أجريت دراسة معمليه على سريان الماء ومحاليل مخففه من البوليمر بتركيز $C = 1, 5, 20, 50, 100$ wppm من مادة البولياكريلاميدا فى وسط مسامى مكون من أنبوبة دائرية المقطع بقطر 20mm ومحشوة بكرات من الصلب بأقطار 3.2 mm وأجريت مقارنه مع النتائج العددية أظهرت تطابقا جيدا أثبتت صحة هدا النموذج.

Abstract:

This work presents an analysis of a non-Newtonian drag reducing fluid (dilute polymer solutions) in a circular pipe filled with porous media. The flow m[illegible] is developed by modifying the momentum equation for the flow in porous media to account for the elongational viscosity of drag reducing fluids. The modified Darcy-Forschheimer-Brinkman's equation is solved using the finite difference method. The results are obtained for flow Reynolds number up to 10^5, a non-Newtonian drag parameter range of $0 \leq \psi \leq 5000$, and nondimensional pressure gradient B up to 10^{10}. The results show that the non-Newtonian effects of drag reducing fluids have a significant influence on the velocity profiles. A very low polymer concentration can cause great reduction in the mean velocity and signifies relative increase in the magnitude of the velocity in the region adjacent to the wall which in turns signifies the channeling effect. This phenomena is reflected in the great influence on the fluid flow characteristics such as the boundary frictional drag, the elongational viscous drag, and in turns in the total drag. Important results documenting and analyzing the behavior of the velocity and the fluid flow characteristics and its

---

Accepted July, 6, 1996

dependence on the non-Newtonian drag parameter are also reported in the course of the study. An experimental investigation was carried out for the flow of water and a dilute polymer solutions with concentrations C = 1, 5, 20, 50 and 100 wppm of the polyacrylamide in a circular tube of 20 mm diameter filled with 3.2 mm diameter stainless-steel spheres. Comparisons of the numerical results with the experimental results show good agreement of the presented results and prove the validity of the model.

1. Introduction

Fluid flow through porous media has been of continuous interest for the past five decades. This interest stems from the complicated phenomena associated with the flow process in porous media, and its very wide applications available. Such applications can be found in chemical engineering, environmental protection, thermal insulation, grain and coal storage, underground water hydrology, drying technology, transpiration cooling, solid matrix heat exchanger, ceramic processing and catalytic reactors. Consequently, understanding the associated transport processes is of critical importance.

The majority of the existing studies were concerned with the Newtonian fluid flow and heat transfer in porous media [1-5]. In fact many industrial processes involve non Newtonian fluid flows with drag reduction characteristics through porous medium such as in oil and chemical industries. From the point of view of drag reduction, the flow of drag reducing polymer solutions in porous medium is very interesting. In fact as the fluid flows through a porous medium it encounters continuous contractions and expansions, and the flow is also subjected to acceleration as well as deceleration and elongational stresses appear. In such flow situations, elastic and non-Newtonian effects of dilute polymer solutions occur when the relaxation time of the fluid exceeds the time scale of the flow. The fluid, then, will not accommodate the flow changes and an increase in the flow resistance will be noted. Such increase is interpreted as an increase in the elongational viscosity due to stretched polymer molecules [6]. Most of the studies were concerned with investigating elongational flows of concentrated polymer solutions. Flow fields such as in expanding jet, through orifice, between cylindrical rollers and through porous medium were experimentally studied. A review for the experimental and analysis of concentrated polymer solutions in such elongational flow fields were done by Savins [7]. The work of Dauben and Menzie [8] was the first to study the flow of dilute polymer solutions through porous medium. This was followed by the work of James and McLaren [9]. Experiments similar to theirs were carried out by Elata et al. [10] and Naudascher and Killen [11]. Elata et al. [10] carried out their experiments using solutions of different concentrations of Polyox Coagulant flowing through porous beds of spherical particles under laminar flow conditions. Laufer et al. [12] studied the flow behavior of two dilute polymer solutions, Polyox WSR 301 and Separan AP 273, at concentrations as low as 25 wppm through porous beds of spherical particles. Rabie et al [6] studied experimentally the flow of dilute polyacrylamide solutions at concentrations up to 50 wppm through porous medium of irregular shape particles (sand) from 0.25 to 4 mm in diameter under laminar, transient and turbulent flow conditions. Yu et al. [13] investigated the flow of two power law fluids through a fixed bed of plastics cubes. Kumar and Upadhyay [14], on the other hand, carried out experiments with one mildly non-Newtonian test liquid through a bed of glass cylinders. Chhabra and Srinivas [15] investigated experimentally the effects of the particle shape on the behavior of the non-Newtonian (purely viscous) fluid flow through packed beds. An extensive measurements on pressure drop in fixed beds, minimum fluidization velocity and expansion characteristics was done by Sharma and Chhabra [16] for beds of non-spherical particles and by Srinivas and Chhabra[17] for beds of spherical particles. It is therefore, safe to conclude that very little is known about the effects of non-Newtonian fluid behavior on the frictional resistance to the flow in porous media and fixed beds.

The object of this paper is to give an analysis for the flow of non-Newtonian drag reducing fluids in a circular pipe filled with saturated porous media (packed sphere beds), taking into consideration the variable porosity, flow inertia, and viscous friction. Also to show the non-Newtonian fluid effects on the fluid velocity and fluid flow characteristics such as the boundary frictional drag, the bulk frictional drag induced by the solid matrix (designed as Darcy's pressure drop), the flow inertia drag induced by the solid matrix at high flow rates (designed as Forschheimer's form drag) and the bulk frictional drag induced by the elongational viscosity due to stretched polymer molecules.

2. Mathematical Formulation

In order to formulate the problem, a steady, hydrodynamically fully developed fluid flow in a horizontal circular pipe filled with packed spheres as a porous medium is considered. It is assumed that the fluid and the solid matrix are in local thermal equilibrium and that the magnitudes of the physical properties such as the viscosity and density are constant. The physical configuration of the problem is shown in Fig. (1) .

As the fluid flows through porous medium, it encounters continuous contractions and expansions, hence, elongational stresses appear. In such flow situations, elastic and non-Newtonian effects of drag reducing fluids occur even for very dilute solutions. This is attributed to the fact that when the relaxation time of the fluid exceeds the time scale of the flow, the fluid will not accommodate the flow changes and an increase of the flow resistance will be noted. Such increase in flow resistance is interpreted as an increase in the elongational viscosity. Therefore, the normal stress in the mean flow direction can be written as [6]

$$\sigma_{11} = -P + (2\mu+\eta)\, G \qquad (1)$$

where, P is the isotropic pressure, G is the streamwise strain rate (du/dx) which is assumed to be proportional to the velocity in the axial direction "u" and η is the elongational viscosity contributed by the presence of polymer molecules in the flow. Equation (1) shows clearly that the increase in flow resistance of porous media due to elastic and non-Newtonian effects of polymer molecules is proportional to "η u". Therefore, the pressure drop per unit length ΔP of polymer solution flow in a porous medium is derived by Rabie et al [6] as:

$$\Delta P = \mu u / \gamma + A \rho u^2 + \eta u / \beta \qquad (2)$$

This equation represents a modified form for Ergun equation for the flow of polymer solutions. $\mu u/\gamma$, $A\rho u^2$ and $\eta u/\beta$ represent the flow resistance due to viscous, inertia, and elastic and non-Newtonian effects respectively.

Accordingly, the Darcy-Forschheimer-Brinkman's equation can be modified for the non-Newtonian drag reducing fluids flow in porous media and written in cylindrical coordinates as:

$$1/\rho . [\partial P/\partial x] = \upsilon / r . [\partial / \partial r (r \, \partial u / \partial r)] - \upsilon u / \gamma - A u^2 - \upsilon u / \beta \qquad (3)$$

where, ρ, υ are the fluid density and dynamic viscosity respectively. γ and A are the permeability and the inertia coefficient (Forschheimer function) of the porous medium, which are dependent on the porosity "ε" and other geometrical parameters of the medium. These parameters are given by Ergun [18] for backed beds of identical spherical particles of diameter "d" and porosity "ε" as;

$$\gamma = d^2 \varepsilon^3 / [175 (1-\varepsilon)^2] \qquad (4)$$

$$A = 1.75 (1-\varepsilon) / [d \, \varepsilon^3] \qquad (5)$$

The first, second, and third terms on the right hand side of equation (3) are expressions for the boundary viscous drag, Darcy frictional drag which is responsible for the porous structure and inertia drag.

The term $(\upsilon . u/\beta)$ on the right hand side of equation (3) represents the elastic and non Newtonian contribution in the total resistance, where β is another drag parameter that depends upon the porous media's geometry (d and ε) as well as the polymer type and concentration.

$$\beta = d^2 \varepsilon^3 / [\psi (1-\varepsilon)^2] \qquad (6)$$

and ψ is a non-Newtonian drag parameter which depends upon the polymer type and concentration and was derived by Rabie et al [6] as;

$$\psi = N . (C [\mu])^n \qquad (7)$$

where C is the volume concentration of the polymer molecules which is taken as the mass concentration since the specific gravity of the polymer is 1.0.

[μ] is the intrinsic viscosity which is given by $[\mu] = K . M^{0.78}$

K, N are numerical constants = 0.0125 and 1.069×10^4 respectively [6]

M is molecular weight of polymer; $M = 5 \times 10^6$ for polyacrylamide

n = 0.5 by Elata et al. [10] and Naudascher and Killen [11] for flow through spherical particles porous media.

The present model using equation (6) can be used for the flow of Newtonian fluid ($\psi = 0$) as well as drag reducing fluids ($\psi > 0$) in porous media.

The porosity "ε" was assumed to vary exponentially from the wall according to the following form;

$$\varepsilon = \varepsilon_e \left[1 + b \exp(c . [r_o - r] / d) \right] \qquad (8)$$

where ε_e is the free stream porosity, and the empirical constants b and were chosen similar to that used by Chandrasekhara and Vortmeyer [19] and El Kady et al.[5] among others.

The boundary conditions imposed on the physical system are uniform with respect to the axial coordinate, the computational domain thus comprises of one half of the pipe over which the velocity u = 0 at $r = r_o$, du/dr = 0 at r = 0

Using the dimensionless variables $U = u/(\upsilon/r_o)$, $R = r/r_o$ and $D = d/r_o$, the momentum equation (3) can be transformed to nondimensional form as;

$$U + C_1 . U^2 = \Gamma \cdot B + (\Gamma / R).[\partial / \partial R (R.\partial U / \partial R)] \qquad (9)$$

where, $C_1 = 1.75\, D / [(\psi + 175)(1-\varepsilon)]$,

$\Gamma = D^2 \varepsilon^3 / [(\psi + 175)(1-\varepsilon)^2]$, and

B is a nondimensional pressure gradient = $- dP/dx \,.\, [r_o^3 / \rho \upsilon^2]$

3. Fluid Flow Characteristics

The flow through the porous duct experiences the boundary frictional drag "f_V", a bulk frictional drag induced by the solid matrix (designed as Darcy's pressure drop) "f_D" and a flow inertia drag "f_I" induced by the solid matrix at high flow rate (designed as Forschheimer's form drag). These factors can be defined [5,20] after changing the variables to our notations and definitions as follows:

$$f_V = \tau_w / [\tfrac{1}{2} \rho u_f^2] \qquad (10)$$

$$f_D = \mu\, \gamma_m^{-1} \varepsilon_m\, u_f\, (r_o/2) / [\tfrac{1}{2} \rho u_f^2] \qquad (11)$$

$$f_I = 0.143\, \rho\, \gamma_m^{-0.5} \varepsilon_m^{0.5}\, u_f^2\, (r_o/2) / [\tfrac{1}{2} \rho u_f^2] \qquad (12)$$

where τ_w is the mean wall shear stress,

u_f is the average local velocity in the x-direction in void volume,

γ_m is the permeability based on the area mean porosity ε_m, and

ε_m is the area mean porosity $\varepsilon_m = [1/r_o^2] \cdot \int_0^{r_o} 2\, r\, \varepsilon\, dr$

In addition to the three parts of the frictional drag in the Newtonian fluid flows, the flow of the non Newtonian drag reducing fluids through the porous ducts experiences also a bulk frictional drag induced by the elongational viscosity due to stretched polymer molecules "f_p". Owing to equation (3) the elongational viscosity drag "f_p" is defined similar to the Darcy frictional drag "f_D" as;

$$f_p = \mu\, \beta_m^{-1} \varepsilon_m\, u_f\, (r_o/2) / [\tfrac{1}{2} \rho u_f^2] \qquad (13)$$

The total bulk drag which is the summation of the four drag types is defined as:

$$f_t = -(dP/dx).(r_o/2)/[\tfrac{1}{2}.\rho u_f^2] \quad (14)$$

Equations (10) - (14) can be written as a function of the nondimensional parameters as:

$$f_V = 8.(dU_f/dR)\big|_{r_0} /Re_f^2 \quad (15)$$

$$f_D = \tfrac{1}{2} . Da^{-1} . Re_f^{-1} \quad (16)$$

$$f_i = 0.0715\, Da^{-0.5} \quad (17)$$

$$f_P = \tfrac{1}{2} . (\psi/175)\, Da^{-1}/ Re_f \quad (18)$$

$$f_t = f_V + f_D + f_i + f_P = 4\, B /Re_f^2 \quad (19)$$

where, Da is the modified Darcy number = $\gamma_m / (4\, r_o^2\, \varepsilon_m)$, and
Re_f is the Reynolds number based of the velocity u_f, $Re_f = 2\, u_f . r_o/ \upsilon$

4. Method of Solution

The non dimensional form of momentum equation (9) is solved numerically to predict the velocity field. The problem is symmetrical with respect to the centerline. therefore, only the top half of the channel needs to be considered. A variable grid in the R direction is employed. The R domain is discritized into 181 grid points to get an accurate solution of the important near-wall region which is used to obtain the momentum equation finite difference form. Equation (9) was transformed into algebraic finite difference equations, following the procedure developed by Patankar [21]. Both the first and second order derivatives in the momentum equation (9) were discretized by using central difference formulas [22]. The Forschheimer nonlinear term is linearized by guessing initial valued of the velocity field at all the grid points, and the nonlinear term was written as the product of the unknown velocity and the guessed velocity. The difference algebraic momentum equation is solved using the Gauss-elimination method to yield the velocity field. Once the velocity profile is known the different drag forms are determined from equations (15-19). .

5. The Experimental Work:

An experimental study for the flow in a porous media is carried out. A schematic diagram of the test rig is shown in Fig. 2. The fluid stored in an overhead tank, 200 liters capacity supplies a small constant head overflow tank 6.0 m above the test section. The fluid flows from the overflow tank under gravity action. The test section is made of a copper tube of 20 mm inside diameter and 250 mm long. The tube is filled uniformly with stainless steel spheres of uniform size to form a packed bed to serve as the solid porous matrix through which fluid flows. The stainless steel spheres are held in place by means of wire mesh located at the two ends of the tube. Spheres of 3.2 mm in diameter are used through out this work. The porous section is kept horizontal in the gravitational open flow system. During the experiments the flow rate varied from 9.42×10^{-6} to 166×10^{-6} m^3/s. A calibrated orifice-meter is used as a flowmeter to measure the high flow rates and

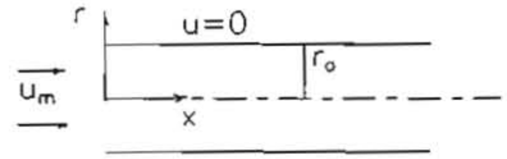

Fig. 1 Physical model, coordinate system and boundaries

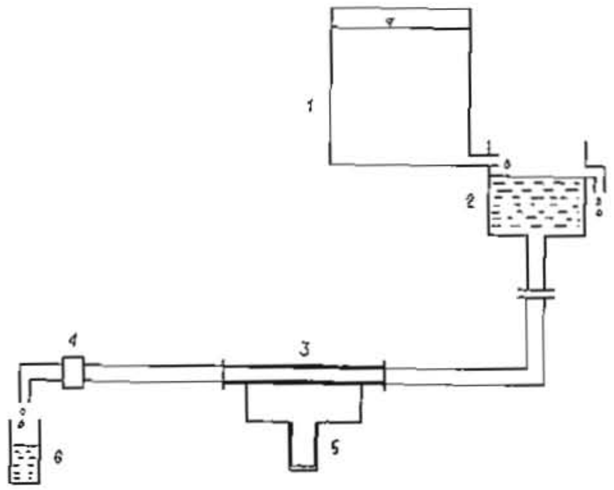

1. Overhead tank
2. Constant head tank
3. Test section
4. Flow meter
5. U-tube manometer
6. Collecting flask

Fig. 2 Schematic diagram of the experimental apparatus from which the mean velocity and Reynolds number of the flow were calculated. For the small flow rates the outlet flow was collected into a four liter flask. The time of filling this tank was measured and the flow rate was calculated. A U-tube mercury manometer is connected to two pressure taps located just upstream and downstream of the test section to measure the pressure drop along the test section. The experiments were performed carefully, each time the experiments were initiated at the largest flow rates; the objective was to produce a stable packing of the beads and to prevent the effects of changing porosity on the pressure drop as the flow rate was varied. The experimental work was done by carrying out series of measurements of pressure drop and flow rate using either water flow or dilute polyacrylamide solutions at concentrations 1,5,20, 50 and 100 wppm.

6. Results and Discussion

6.1 Flow Velocity and Channeling

The velocity distribution across the pipe including the channeling effect is the main driver for the behavior of the flow characteristics of drag reducing fluids in a porous media. To explain the variation of flow parameters due to the change of the polymer concentration, the velocity distribution and the channeling effect are studied.

Figures 3 and 4 show the behavior of the flow velocity U and the ratio U/U_o along the pipe half section for a variation of ψ from 0 to 3000 where C = 37 wppm, d = 3.2 mm, D = 0.32 and B = 10^4. Where U_o is the velocity of the flow for the case of $\psi = 0$. Figure 3 shows a remarkable reduction of the velocity near the wall and in the core with increase of ψ (increase of polymer concentration), while figure 4 presents the following:

- The case of ψ = 175 which corresponds to nearly a concentration of 0.125 wppm of polyacrylamide, causes a reduction in the flow velocity in the core of about 50% with a sudden and sharp decrease to about 23% in the layer adjacent to the wall, while for a concentration of about 1 wppm which corresponds to ψ = 500, a reduction in the flow velocity of the core is about 74% with a sudden and sharp decrease near the wall to about 50% of the velocity of the Newtonian fluid flow. This means that very low polymer concentrations which have no detectable effects on the physical properties, can cause great changes in the velocity distribution..
- The thickness of the layer near the wall at which the sudden and sharp decrease of the velocity occurs, decreases with the increase of ψ (polymer concentration)
- The increase of ψ decreases the flow velocity in the core with a higher rate than that near the wall, i.e. the rate of velocity reduction in the layer adjacent to the wall increases with the increase of the distance from the wall until the core of the flow where the velocity is then constant

Figure 5 pertains the distribution of the velocity U/U_m across the pipe half section with the variation of ψ, where U_m is mean flow velocity. This figure shows the changes of the channeling effect and the velocity values near the wall relative to the mean flow velocity due to the variation of ψ. It clearly shows the following:

- U/U_m decreases in the core with the increase of ψ, while it increases near the wall, i.e. in the region adjacent to the wall the channeling effects increases with the increase of ψ

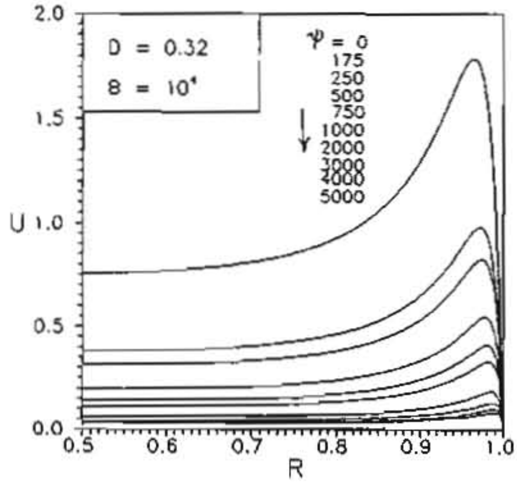

Fig. 3 Velocity distribution U along the tube radius according to Eq. (9) for different values of ψ, $D = 0.32$ and $B = 10^4$

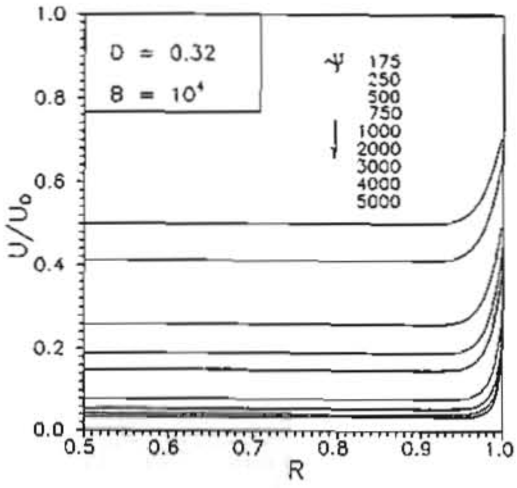

Fig. 4 Velocity distribution U/U_o along the tube radius for different values of ψ, $D = 0.32$ and $B = 10^4$

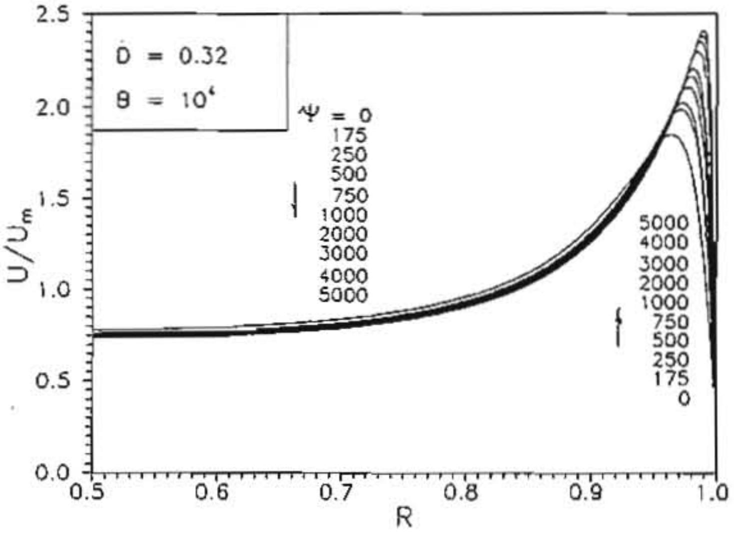

Fig. 5 Velocity distribution U/U_m along the tube radius for different values of ψ, $D = 0.32$ and $B = 10^4$

- With the increase of ψ, the point of the maximum channeling velocity deviates towards the wall.

Such changes in velocity distribution are attributed to the fact that, the increase of the polymer concentration (increase of ψ) increases the relaxation time of the fluid which makes it unable to accommodate the flow changes, and the continuous contractions and expansions of the porous surface. As the void volume increases with the direction towards the wall, the rate of continuous contractions and expansions of the porous surface decreases, which decreases the elongational stresses and makes the fluid flows faster near the wall and the point of the maximum channeling velocity deviates towards the wall.

6.2 Flow Characteristics

The fluid flow is characterized by the friction factors f_v, f_d, f_i, f_p and f_t which are described by equations (15-19). The total friction factor f_t depends mainly on both Reynolds number Re, and the nondimensional pressure gradient B. To show the effect of the polymer concentration on f_t, it is very useful to know first the relation between both the superficial velocity and the pressure drop in the non-dimensional form i.e. Re and B where $Re = 2u_m.r_o/\upsilon$. Figure 6 shows the behavior of the nondimensional calculated pressure gradient B (which is an indication of the filtration resistance) with the change of Reynolds number for $d = 3.2$, $D = 0.32$ and a range of $0 \leq \psi \leq 4000$. Figure 6 presents the linear increase of B in the logarithmic graph until nearly Re = 100, where the curves start to converge towards one curve. They coincide at $Re \geq 5x10^4$. In the region of $Re \leq 100$, an increase occures in B of about 3 times that of the Newtonian fluid for $\psi = 250$ which corresponds to nearly 0.25 wppm of polyacrylamide. For $\psi = 1000$ ($C \approx 4$ wppm of polyacrylamide) that increase is about 10 times that of the Newtonian fluid. Such very low polymer concentrations, which have no detectable effects on the physical properties of the Newtonian fluid, can cause serious problems to filtration processes.

For constant non dimensional pressure drop B the Reynolds number decreases sharply with the increase of ψ as shown in figures 7and 8. Figure 8 presents the ratio of Re/Re_o with the increase of ψ for three cases of $B = 10^4$, $5x10^4$ and 10^5. The three cases coincide together in nearly one curve. For $\psi = 175$ ($C = 0.125$ wppm of polyacrylamide), Re/Re_o takes the value 0.52, which means a reduction in Re of 48%. For $\psi = 500$ (C=1 wppm of polyacrylamide), Re/Re_o takes the value 0.28, which means a reduction in Re of 72%. For an increase in ψ from 2000 to 4000, i.e. increase of C from 17 to 70 wppm only a reduction in Re of about 4% occurs. Three types of Re/Re_o behavior with ψ are exhibited. They are, sharp decrease in Re/Re_o for $\psi \leq 500$, transient decrease for $500 \leq \psi \leq 3000$ and nearly constant Re/Re_o for $\psi \geq 3000$.

Figure 9 presents the variation of the total friction factor f_t with Re for $d = 3.2$, $D = 0.32$ which corresponds to $Da = 6.2x10^{-5}$ and a range $0 \leq \psi \leq 4000$. The (f_t -Re) curves take linear shape in the laminar region, curved shape in the transient and constant value for the turbulent regions. With the increase of ψ the total friction factor f_t increases due to the presence of the elongational viscosity drag f_p. Figure 10 shows the relative increase of the total friction factor due to the polymer additives with the increase of Re (f_t/f_{to} -

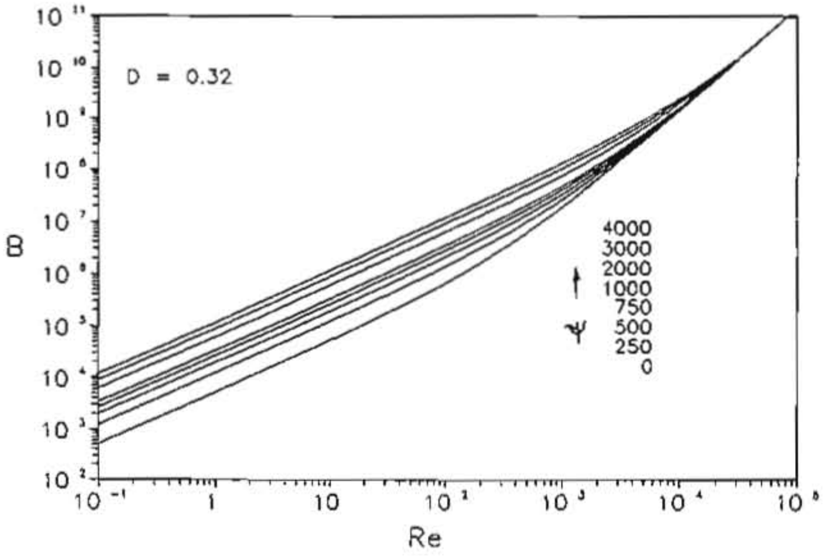

Fig. 6 Dependence of the nondimensional pressure drop B on Re for a host values of ψ and $D = 0.32$

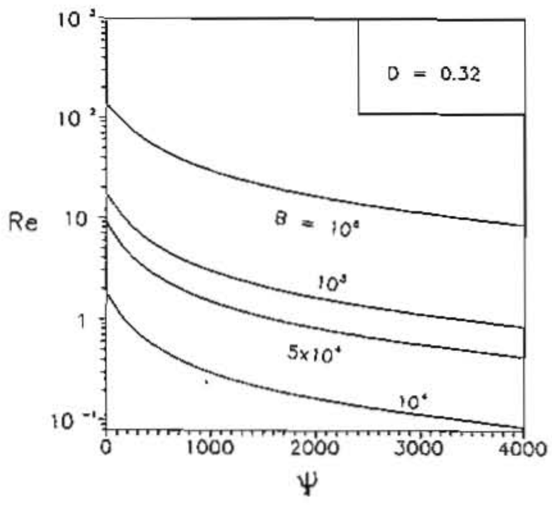

Fig. 7 Re - ψ diagram for different values of B and $D = 0.32$

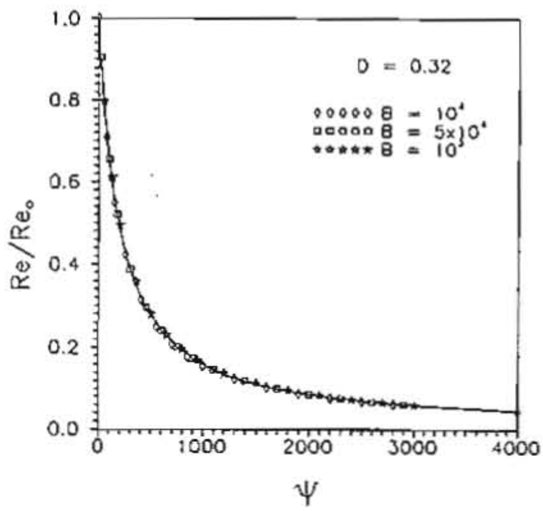

Fig. 8 Re/Re_o-ψ diagram for different values of B and $D = 0.32$

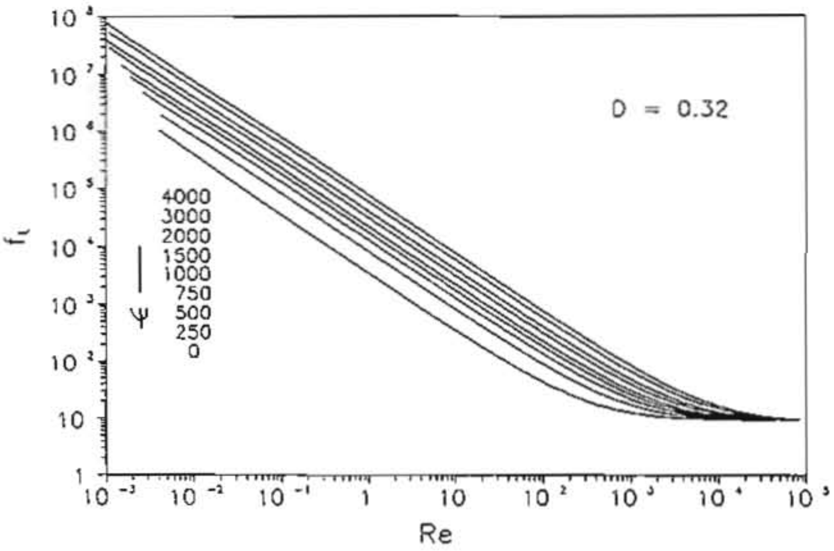

Fig. 9 Total friction factor f_t variation with Re for a host values of ψ and $D = 0.32$

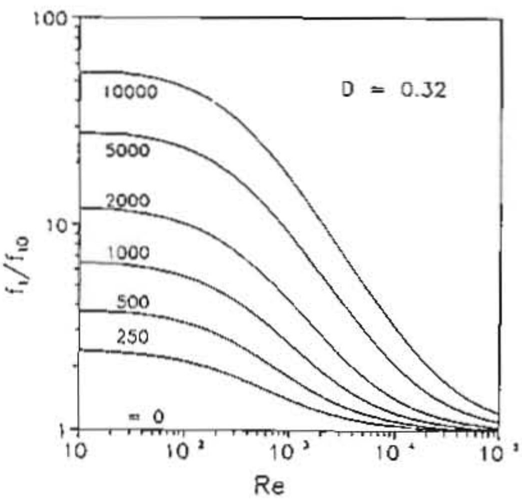

Fig. 10 Total friction factor ratio f_t/f_{to} variation with Re for a host values of ψ and $D = 0.32$

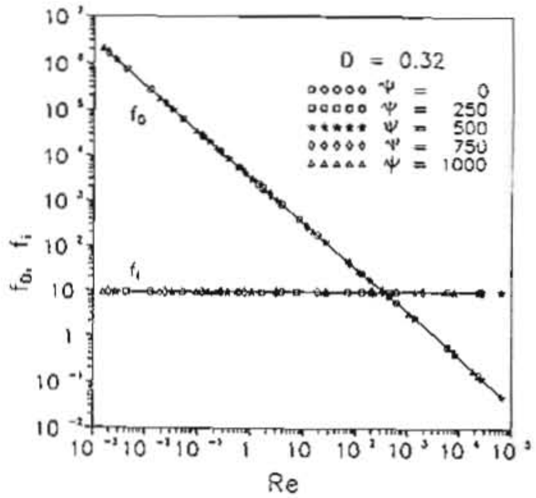

Fig. 11 Friction factors f_D and f_i variation with Re for a host values of ψ and $D = 0.32$

Re), where f_{to} is the total friction factor in the case of ψ=0. There are also three types of behavior for f_t. Sharp and linear decrease in f_t for Re ≤ 100, transient decrease for 100 ≤ Re ≤ 5x10^4 and nearly constant f_t for Re ≥ 5x10^4

The behavior of the Darcy friction f_D, inertia friction f_i, the boundary viscous drag f_v and the elongational viscosity drag f_p with Reynolds number Re are presented in Figs. 11-13 for d=3.2mm, D = 0.32 and a range of 0 ≤ ψ ≤ 4000. The results show the following;

- f_i is independent on Re, f_D is changed linearly in the logarithmic graph with Re and both f_i and f_D are independent on ψ.
- f_v shows an increase with ψ in Figs. 12 and 13. Because f_v is a function of the velocity gradient at the wall boundary, the increase of polymer concentration, (increase of ψ, and decrease of β) yields to an increase in f_v due to the increase of the velocity gradient near the wall as shown in Figs. 3 and 4.
- f_p decreases linearly in the logarithmic graph with Re and increases with ψ. From equations 16 and 18 "$f_p = (\psi/175).f_D$", hence, (f_p <=> f_D) by (ψ <=> 175).

Figure 14 shows the total friction factor f_t and the four parts of it, i.e. the Darcy's friction f_D, inertia friction f_i, the boundary viscous drag f_v and the elongational viscosity drag f_p with Reynolds number Re, while Fig. 15 presents the contribution of each of the different friction factors f_D/f_t, f_v/f_t, f_p/f_t and f_i/f_t in the total friction for d=3.2 mm, D = 0.32 and ψ = 1000. Three regions for the behavior appear in Figs. 14 and 15:

- Re≤100. f_i/f_t is negligible, $f_p/f_t = (1000/175) f_D/f_t$ and shares with the main part.
- 100 ≤ Re ≤ 5x10^4 Transition region in which the three types of friction factors f_D/f_t, f_v/f_t, f_p/f_t decrease sharply while the inertia friction factor f_i/f_t increases sharply
- Re ≥ 5x10^4. f_t curve overlaps with the line of f_i, the three types of friction f_D/f_t, f_v/f_t and f_p/f_t are neglected and f_i/f_t asymptotes to the value 1. i.e. the flow depends mainly on the inertia friction f_i which is constant with Re. This facts gives the reason for the no change in the behavior of B with Re with the increase of ψ which is shown in Fig. 6.

Figures 16-19 show the behavior of the inertia friction factor f_i/f_t, the Darcy's friction f_D/f_t, the elongational viscosity drag f_p/f_t and the boundary viscous drag f_v/f_t with the variation of Re in the three regions for d=3.2 mm, D = 0.32 and values of ψ = 0, 250, 500, 750, 1000, 2000, 3000 and 4000. The figures show the increase of the elongational viscosity drag f_p/f_t and the decrease of the three other parts of the friction factors which belongs to the Newtonian fluid flow with the increase of ψ along the three regions of the flow.

To validate the numerical model developed in this work, the pressure drop and the volume flow rate are experimentally measured, and both Reynolds number and the total friction factor were calculated and compared with the numerical results. Figure 20 presents the comparison between the experimental and numerical values of the total friction factor with the change of Reynolds number for spherical sized packed beads of d=3.2 mm diameter and for different five polymer concentrations with C = 1, 5, 20, 50 and 100 wppm of the polyacrylamide. These concentrations are corresponding to ψ = 490,

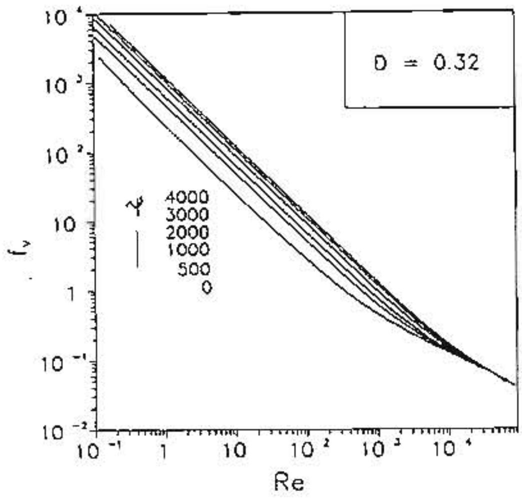

Fig. 12 Friction factor f_v variation with Re for a bost values of ψ and $D = 0.32$

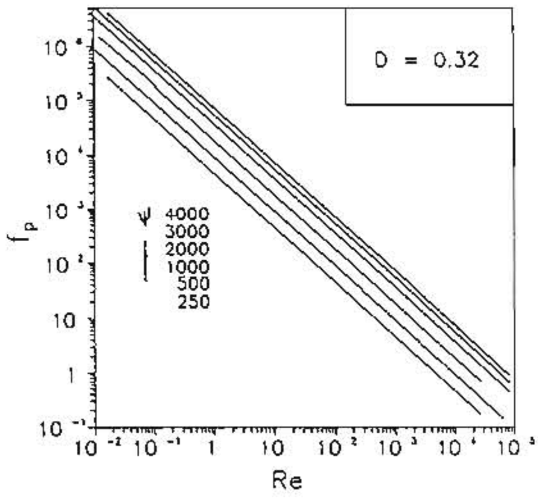

Fig. 13 Friction factor f_p variation with Re for a bost values of ψ and $D = 0.32$

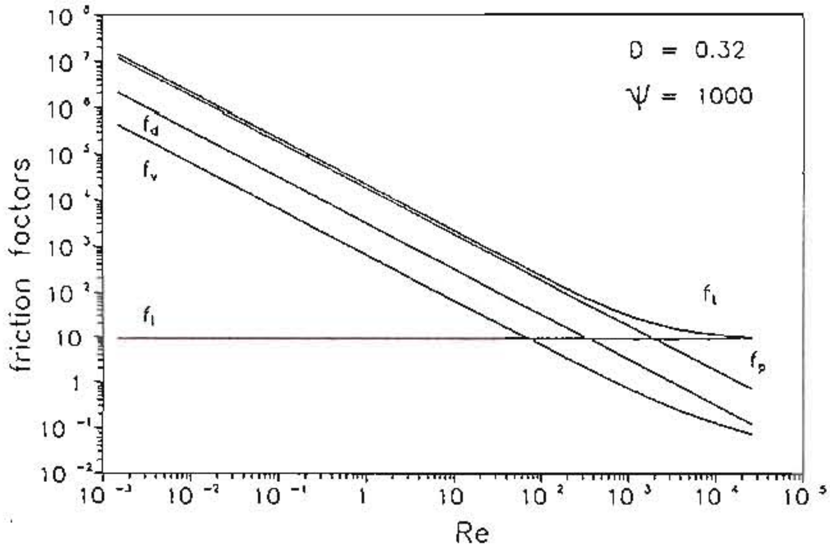

Fig. 14 Friction factors f_t, f_D, f_v, f_i and f_p variation with Re for ψ = 1000 and $D = 0.32$

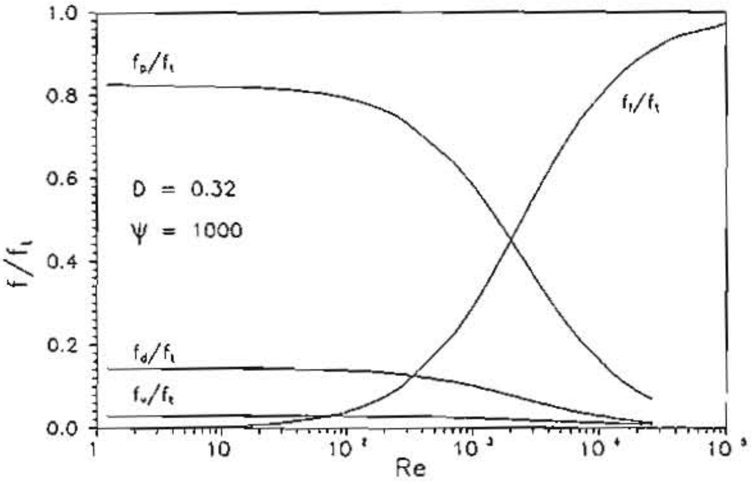

Fig. 15 Friction factors f_D/f_t, f_V/f_t, f_i/f_t and f_p/f_t variation with Re for $\psi = 1000$ and $D = 0.32$

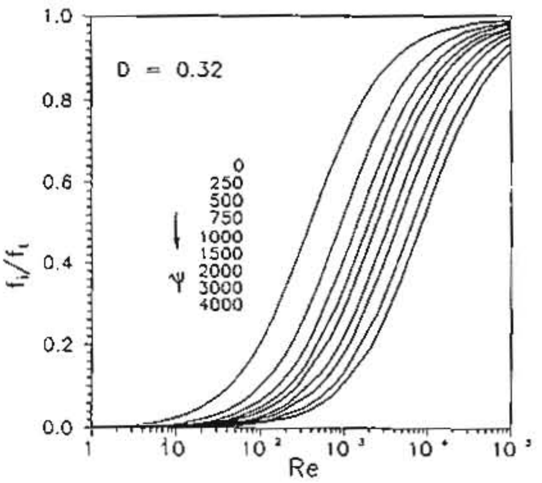

ig. 16 Friction factor f_i/f_t variation wit Re for a host values of ψ and $D = 0.32$

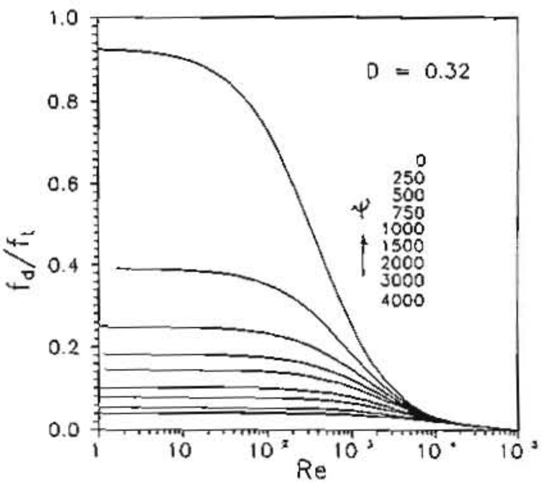

Fig. 17 Friction factor f_D/f_t variation wit Re for a host values of ψ and $D = 0.32$

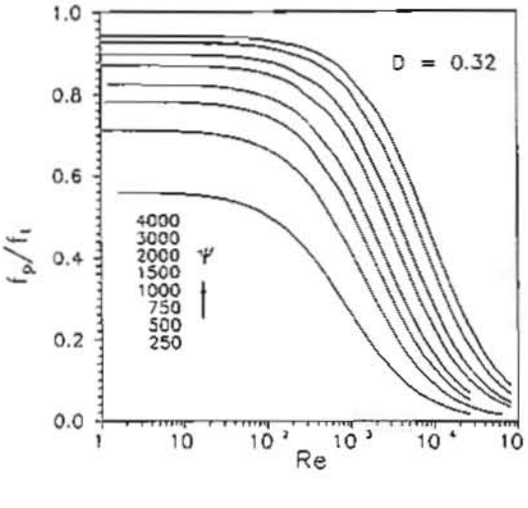

ig. 18 Friction factor f_p/f_t variation with Re for a host values of ψ and $D = 0.32$

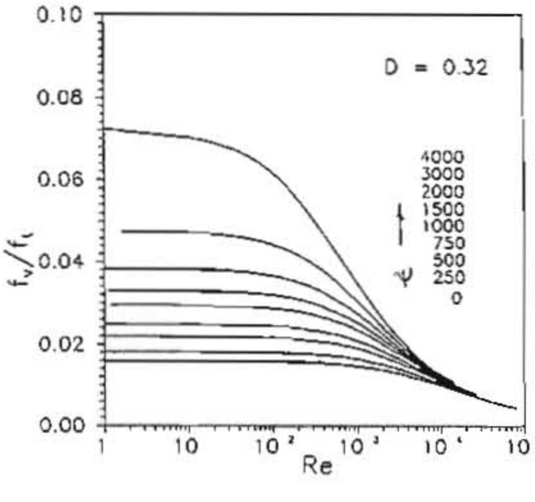

Fig. 19 Friction factor f_v/f_t variation wit Re for a host values of ψ and $D = 0.32$.

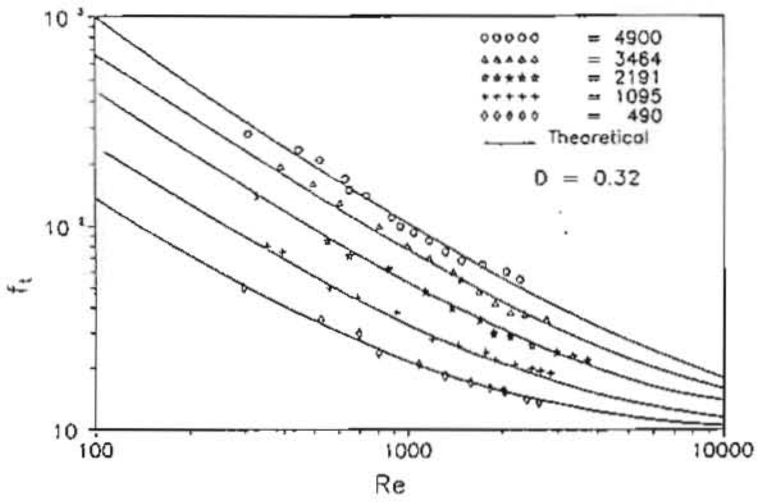

Fig. 20 Total friction factor f_t versus Reynolds number Re for different values of ψ, and $D = 0.32$. Comparison with the experimental results

1095, 2191, 3464 and 4900 respectively. The comparison shows good agreement of the presented results and proves the validity of the model.

7. Conclusions

Non-Newtonian drag reducing fluid flows in a circular pipe filled with porous media are analyzed. The effects of the fluid elongational viscosity on the fluid velocity and fluid flow characteristics are presented. In modeling the flow, the variable porosity, flow inertia, Brinkman viscous friction and the elongational viscosity (non-Darcian effects) are taken into account. A modified Darcy-Forschheimer-Ergun flow model and the finite difference method are applied. It can be concluded that the non-Newtonian effects of drag reducing fluids have a significant influence on the velocity profiles, the pressure drop, the Reynolds number Re and the total friction f_t as following;

- Very low polymer concentrations can cause great reduction in the mean velocity and signifies relative increase in the magnitude of the velocity in the region adjacent to the wall which in turns signifies the channeling effect.
- At constant Reynolds number Re, the increase of ψ causes an increase in the nondimensional pressure drop B until Re is nearly $= 5\times10^4$ where the elongational viscosity drag f_p effect disappears and no effect of ψ will be noticeable
- For constant pressure gradient, the behavior of flow Re with polymer concentration and type drag parameter ψ exhibits three different regions namely, sharp decrease in Re for $\psi \le 500$, transient decrease for $500 \le \psi \le 3000$ and constant Re for $\psi \ge 3000$.
- Three different regions in the behavior of f_t with Re are found. Sharp linear decrease in f_t for $Re \le 100$, transient decrease in f_t for $100 \le Re \le 5\times10^4$ and nearly constant value of f_t for $Re \ge 5\times10^4$. With the increase of ψ the total friction factor f_t increases due to the effect of the elongational viscosity drag f_p until $Re \ge 5\times10^4$ where this effect disappears and no effect of ψ is noticeable
- The elongational viscosity drag f_p decreases linearly in the logarithmic scale with Re and increases with ψ. "$f_p = (\psi/175).f_D$", so ($f_p <=> f_D$) by ($\psi <=> 175$).
- The increase of the polymer concentration and type drag parameter ψ, causes an increase in the velocity gradient near the wall which in turns increases the boundary viscous drag f_v while, both the inertia friction f_i and the Darcy's friction f_D are independent on ψ.

8. Nomenclature

A	Forschheimer inertia coefficient of the porous medium, equation (2), m^{-1}
b, c	constants, equation (8)
B	nondimensional pressure gradient , equation (9)
C	concentration of the polymer molecules equation (7); in wppm
C_1	dimensionless coefficient, equation (9)
d	sphere diameter, m
D	dimensionless sphere diameter = d/r_o
Da	modified Darcy number = $\gamma_m/(4r_o^2.\varepsilon_m)$

f_D frictional drag factor (Darcy's pressure drop)
f_i flow inertia drag induced by the solid matrix
f_p elongational viscosity drag factor
f_t total drag factor
f_v boundary viscous friction factor
K numerical constant = 0.0125
M molecular weight of polymer = 5×10^6 for polyacrylamide
n, N numerical constants equation (5)
P pressure, Pa
r radial coordinate
r_o pipe radius, m
R dimensionless radial coordinate
Re Reynolds No. based on the velocity u_m, $Re = 2u_m . r_o/\upsilon$
Re_f Reynolds No. based on the velocity u_f, $Re_f = 2u_f . r_o/\upsilon$
u field velocities in the x direction, m/s
U non-dimensional field velocities in the X direction = $u/(\upsilon / r_o)$
u_f local average velocity in the x-direction in void volume = u_m/ε_m
u_m local averaged fluid velocity including the solid and fluid regions
x axial coordinate
β non-Newtonian drag parameter equation (4).
γ permeability of the porous layer, equation 2, m^2
γ_m permeability based on the area mean porosity ε_m
Γ dimensionless coefficient, equation (7).
ψ type drag parameter equation (5).
ε porosity of the porous medium
ε_e free-stream porosity
ε_m area mean porosity
τ_w mean wall shear stress, N/m^2
$[\mu]$ intrinsic viscosity; $[\mu] = K.M^{0.78}$
υ kinematic viscosity of the fluid, m^2/s
ρ fluid density, kg/m^3

9. References

1. Vafia, K., Alkire, R. L., and Tien, C. L., " An Experimental Investigation of Heat Transfer in Variable Porosity Media," ASME Journal of Heat Transfer, Vol. 107, pp. 642-647, 1985.
2. Kaviany, M., "Laminar Flow Through a Porous Channel Bounded by Isothermal Parallel Plates," Int. J. of Heat and Mass Transfer, Vol. 28, pp. 851-858, 1985.
3. Poulikakos, D., and Renken, K., "Forced Convection in a Channel Filled With Porous Medium, Including the Effects of Flow Inertia, Variable Porosity, and Brinkman Friction," ASME, Journal of Heat Transfer, Vol. 109, pp. 880-888, 1987.
4. Cheng, P., Hsu, C. T., and Chowdhury, A., "Forced Convection in the Entrance Region of a Packed Channel With Asymmetric Heating," ASME Journal of Heat Transfer, Vol. 110, pp. 946-954, 1988.

5. El Kady, M.S., Tolba, M. A. and Rabie, L. H., "Flow in a Circular Pipe Filled With Porous Medium in the non-Darcian Effects," To be Published.
6. Rabie, L. H., Arid, F. F., and Shalaby, M. A., " Flow of Dilute Polymer Solutions in Porous Media" Mansoura Engineering Journal. Vol. 11, No 2, pp. M85-M95, December 1986.
7. Savins, J. G., "Non-Newtonian Flow Through Porous Media". Industrial Engineering Chemistry, Vol. 61, pp. 18-47, 1969.
8. Dauben, D. L., and Menzie, D. E., Journal of Pet. Technology, 240. 1065, 1967.
9. James, D. F., and McLaren. D. R., J. of Fluid Mechanics, Vol. 70, pp. 733, 1975
10 Elata, C., Burger, J., Michelin, J., and Takserman, U., Physics of fluids. vol. 20, pp. 49, October part II, 1977.
11. Naudascher, A. and Killen, J. M., Physics of fluids, Vol. 20, pp. 280, October part II. 1977.
12. Laufer, G., Gutfinger, G., and Abuaf, Ind., Eng. Chem. Foundam., Vol. 15, pp. 77, 1976.
13 Yu, Y. H., Wen, C. Y., and Bailie, R. C., "Power Law Fluids Flow Through Multiparticle Systems," Can. J. Chem. Eng. Vol. 46, pp. 149-154, 1968.
14. Kumar, S. and Upadhyay, S. N., "Mass and Momentum Transfer to Newtonian and non-Newtonian Fluids in Fixed and Fluidized Beds", Ind., Eng. Chem. Foundam., Vol. 20, pp. 186-195, 1981.
15. Chhabra, R. P. and Srinivas, B. K.,"Non-Newtonian (Purely Viscous) Fluid Flow Through Packed Beds: Effect of Particle Shape," Power Technology, Vol. 67, pp. 15-19, 1991
16. Sharma, M. K. and Chhabra, R. P., "An Experimental Study of non-Newtonian Fluid Flow Through Fixed and Fluidized Beds of non-Spherical Particles," Can. J. of Chem. Eng., Vol. 70, pp. 586-591, 1992.
17. Srinivas, B. K. and Chhabra, R. P., "An Experimental Study of non-Newtonian Fluid Flow in Fluidized Beds: Minimum Fluidization Velocity and Bed Expansion Characteristics," Chem. Eng. Process, Vol. 29, pp. 121-131, 1991.
18. Ergun, S., "Fluid Flow Through Packed Columns," Chemical Engineering Progress, Vol. 48, pp. 89-94, 1952.
19. Chandrasekhara, B. C., and Vortmeyer, D., "Flow Model for Velocity Distribution in Fixed Porous Beds Under Isothermal Conditions," Th.. Fluid Dynamics, Vol. 12, pp. 105-111, 1979.
20. Hwang, G., and Chao, C., " Effects of Wall Conduction and Darcy Number on Laminar Mixed Convection in a Horizontal Square Porous Channel," ASME J. of Heat Transfer, Vol. 114, pp. 614-621, 1992.
21. Patankar, S., "Numerical Heat Transfer and Fluid Flow" McGraw Hill, New York, 1980.
22. Hirsch, C., "Numerical Computation of Internal and External Flows, Vol 1: Fundamentals of Numerical Discretization" John Wiley & Sons , 1991.